Future hotspots of compound dry and hot summers emerge in European agricultural areas

Andrea Böhnisch[1], Elizaveta Felsche[1,2], Magdalena Mittermeier[1], Benjamin Poschlod[3], Ralf Ludwig[1]

[1]Department of Geography, Ludwig-Maximilians-Universität München, Munich, Germany
[2]Center for Digital Technology and Management, Munich, Germany
[3]Research Unit Sustainability and Climate Risk, Center for Earth System Research and Sustainability, Universität Hamburg, Hamburg, Germany

Key Points:

- During compound dry and hot extreme (CDHE) summers, latent heat flux is markedly reduced in widespread areas of the European continent.
- The frequency increase of CDHE events, associated with extremely low soil moisture, doubles under GWL3 compared to GWL2.
- CDHE frequency increases are predominantly driven by rising temperature, with regional contributions of bivariate tail dependence increases.

Corresponding author: Andrea Böhnisch, a.boehnisch@lmu.de

Abstract

Compound dry and hot extremes (CDHE, such as recent summers 2015, 2018 and 2022 in Europe) have wide ranging impacts: Heat exacerbates moisture shortages during dry periods whereas water demand rises. Climate change will likely increase the intensity, frequency, and duration of CDHE events in Europe. However, current studies focus on drivers and impacts in coarse-resolution global climate models and likely miss spatial details of CDHE characteristics. To overcome this issue, we exploit a regional 50-member single-model initial condition large ensemble (SMILE) at 12 km spatial resolution. Hence 1000 model years per 20 year-periods provide an extensive database of CDHE and robust estimations of their occurrence changes across Europe in high geographical detail. CDHE occurrences are investigated in a current climate and at two global warming levels (+2 °C, +3 °C). We identify Northern France, Southern Germany, Switzerland, Southern Ireland, and the western coasts of the Black Sea with currently low CDHE frequencies as emerging hotspots. These regions experience a tenfold occurrence increase under global warming conditions. Apart from Western Europe, temperature is the dominant contributor to frequency increases. Furthermore, tail dependencies strengthen in regions with high CDHE frequency increases. In European agricultural areas, soil moisture shows very strong negative correlations with CDHE extremeness. Last, our results suggest a halving of CDHE in a +2 °C world compared to a +3 °C world, highlighting the necessity of climate mitigation with respect to this hazard type.

Plain Language Summary

During the last years, summers tended to be exceptionally dry and hot at the same time. Dry and hot conditions affect various economic and ecologic sectors, for example agriculture by soil moisture reduction. Assessing their frequency and intensity under climate change conditions is hence pivotal to develop effective adaptation strategies. The particularity of this study is a so-called regional climate model large ensemble: Its 50 simulations from the same model are equally probable realizations of climate trajectories. We thus investigate 1000 model years for a current climate, a +2°C and +3°C warmer world at high geographical detail. This allows for robust analysis as numerous events occur per period. We show that hot and dry summers become more frequent, mostly because of warming with some regions affected by both warming and drying. Furthermore, we find a strengthening link between high temperature and low precipitation, which is often not considered in studies. Additionally, lower soil moisture conditions in agricultural areas coincide with more extreme dry and hot summers. In a +3°C world, these events are projected to occur at least twice as frequent as in a +2°C world. This stresses the relevance of climate change mitigation efforts.

1 Introduction

Triggered by an accumulation of recent events, the temporal co-occurrence of extremely dry and hot conditions has sparked a large literature body. Globally, but especially in Europe, simultaneous droughts and heatwaves rank first among multivariate hazard investigations (Afroz et al., 2023). Up to 20 % of heatwaves coincided with droughts since the 1980s (rising trend; Mukherjee & Mishra, 2021). In Europe, droughts during the warm season – often accompanied by heatwaves – increasingly emerge as the dominant drought type (Markonis et al., 2021). For instance, the year 2018 exhibited unprecedented dry and hot conditions during spring to summer in the northern hemisphere (Buras et al., 2020). Vegetation, thriving from suitable growing conditions in spring, aggravated soil depletion by summer due to enhanced transpiration (Bastos et al., 2020).

Heatwaves and droughts share common drivers, albeit on different effective time scales (Miralles et al., 2019). This is reflected in the general negative correlation of temperature and precipitation (Zscheischler & Fischer, 2020; Trenberth & Shea, 2005). For

example, in 2018 anticyclonic blocking through April–October over central Europe, in particular a stationary pattern that was recurrently associated with heat anomalies over Europe and North America, favored persistent dry and hot conditions (Buras et al., 2020; Toreti et al., 2019; Rousi et al., 2023; Kornhuber et al., 2019). Buras et al. (2020) also show the close spatial correspondence of high pressure, hot extremes (which typically occur below anticyclonic conditions, Kornhuber et al., 2019), and water budget deficits. This context can be explained by drying and warming in descending air masses, which exacerbate atmospheric evaporative demand such that subsequently increased evapotranspiration may reduce soil moisture (e.g., Zscheischler et al., 2020). Dry soils in turn heat up more quickly and thus support the sensible heat flux (e.g., Schwingshackl et al., 2017). The warming effect in humid areas during hot and dry conditions due to enhanced net radiation is dampened by evaporative cooling, which is induced by vegetation transpiration and soil evaporation (O et al., 2022). In arid areas, generally low soil water contents and dry vegetation constrain latent heat and amplify temperature increases via enhanced sensible heat fluxes (O et al., 2022). Locally, drought conditions precede extreme heat in summers (Felsche et al., 2023), while simultaneous drought conditions may prolong heatwaves via land-atmospheric coupling (Fischer et al., 2007).

This relationship is mutual: Manning et al. (2019) suggest that enduring and intense hot and dry conditions also trigger soil moisture droughts, and Mukherjee et al. (2023) find amplifying soil effects in both drought–heat and heat–drought cascades. In Germany, soil moisture depletion and precipitation deficits during summer 2018 resulted in a shift from commonly energy-limited to moisture-limited evaporative regimes (Rousi et al., 2023). Soil moisture deficits, however, considerably hamper vegetation productivity (Bastos et al., 2020). In summer 2018, the general water budget was more strongly affected in European agricultural and pasture regions than in forests, but vegetation degraded in both arable and forest regions (Buras et al., 2020). Crop yields of major plants in Northern and central Europe were halved compared to the preceding 5 years (Toreti et al., 2019). In the similarly hot and dry summer of 2003, European gross and net primary production decreased by up to 30 % and 20 %, respectively (Ciais et al., 2005). While heat was shown to mostly affect crop yields, droughts additionally kill the plants (Lesk et al., 2016). Thus a co-occurrence of both extremes also bears the potential to merge impacts, especially by affecting soil moisture as a pre-condition for crop development.

The impacts of compounding extremes are hence amplified compared to its single components. This holds also true for compound dry and hot extreme (CDHE) events, as mentioned previously. Literature describes various kinds of compound events, e.g., preconditioned, temporally or spatially compounding, and multivariate types (e.g., Zscheischler et al., 2020). CDHE can be considered as multivariate, in that two hazards co-occur simultaneously in time and space due to their common drivers, or as pre-conditioned if, e.g., soil moisture conditions of previous seasons were taken into account (Zscheischler et al., 2020). Identifying compound events with joint distributions, in this case of temperature and precipitation, allows their investigation via multivariate probability distribution functions, i.e., copulas (Bevacqua et al., 2017; Zscheischler et al., 2020). These represent dependencies among the variables and can be used to derive multivariate extreme value probabilities (Zscheischler et al., 2020). Event occurrence probabilities in turn can be expressed as return periods. For instance, return periods for the CDHE growing season 2018 exceed several thousand years for certain event definitions (Zscheischler & Fischer, 2020). Especially in situations where adaptation and decision making rely on return periods, such as water resources management, bivariate analyses are essential. Without considering the bivariate dependence structure, there is a risk of both overestimating or underestimating the occurrence of events (Bevacqua et al., 2017): For instance, bivariate return periods of the 2014 California winter drought, one of the first CDHE to be investigated bivariately, were shown to be higher than univariate precipitation deficit return periods owing to extremely high winter temperatures (AghaKouchak et al., 2014).

Most studies on bivariate events focus on prominent cases without gaining generalized knowledge on the event–impact relationships by, e.g., aligning event extremeness with impact extremeness. Examples for this approach include the calculation of (standardized) temperature and precipitation ratios or products (Hao et al., 2018; Mukherjee & Mishra, 2021), but without considering the variable dependencies. Others employ water budget deficits as CDHE intensity surrogate (Buras et al., 2020). In this study, we consider bivariate return periods as an intensity surrogate. Since they indicate the joint extremeness of the considered variables, higher return periods also correspond to higher temperatures and lower precipitation in the CDHE case. To illustrate the intensity of the bivariate return periods, we align soil moisture to the CDHE.

In order to evaluate low-frequency compound events and derive meaningful knowledge on their effects on soil moisture, observational records provide too few events. Hence, ensembles of climate model simulations are beneficial to enlarge the event sample. However, for the investigation of compound events, it is advisable to be sure about comparable process representation in all used simulations (e.g., regarding the joint temperature–precipitation distribution). Both issues can be addressed by accessing single-model initial condition large ensembles (SMILEs) (e.g., Maher et al., 2021). SMILEs consist of several simulations of the same model under the same external forcing conditions (i.e., scenario), differing only due to their initial conditions. Global SMILEs proved to be a skillful tool for the reduction of uncertainty due to internal variability in multivariate event attribution (Bevacqua et al., 2023). However, it is a known issue that compound events require finer spatial resolution if realistic information for adaptation planning on a regional scale is sought (François & Vrac, 2023).

The goal of this study is thus to (a) obtain and explain spatially explicit frequency changes in European CDHE summers (June–August, JJA) under three global warming levels and (b) relate the ranked events with soil moisture as a relevant condition for impacts on agriculture. In order to reduce sampling uncertainties from a statistical perspective and address internal climate variability, we employ a regional high resolution SMILE.

2 Materials and Methods

2.1 Regional Large Ensemble Data for robust sampling

Investigating low-probability compound events of extremes requires an abundant data base. We therefore employ the regional SMILE of the Canadian Regional Climate Model, version 5 (CRCM5-LE; Leduc et al., 2019). The CRCM5-LE was developed within the ClimEx project: 50 members of the Canadian Earth System Model, version 2, Large Ensemble (CanESM2-LE; Fyfe et al., 2017; Kirchmeier-Young et al., 2017) were dynamically downscaled with the CRCM5 to obtain 50 high-resolution (0.11 °, corresponding to 12.5 km) time series of 1950–2099 over two domains, Europe and Northeastern North America (Leduc et al., 2019). The original members of the CanESM2-LE were constructed by applying small random perturbations to the long-term control run in 1850 and subsequently in 1950. After a few years, the 50 members are considered to be independent due to the chaotic nature of weather sequences, while still following the same forcing conditions (RCP8.5 from 2006 onward) and thus pertaining comparable climate statistics (Leduc et al., 2019).

The CRCM5-LE already proved its value for compound analyses of hydro-meteorological extremes, namely rain on saturated soil and rain-on-snow events (Poschlod et al., 2020). Further, this regional SMILE was used for investigation of heatwaves (Böhnisch et al., 2023), droughts (Böhnisch et al., 2021), and heat and drought linkage at an inter-seasonal scale (Felsche et al., 2023).

2.2 Global Warming Levels in a regional climate model

We employed global warming levels (GWL) for our analysis of future climate projections. This approach has been widely applied because it has the advantage of being less sensitive to the selected model and scenario. Furthermore, it allows to directly compare the warming rate to the goal of the Paris Agreement of limiting global warming to "(...) well below 2 °C above pre-industrial levels and to pursue efforts to limit the temperature increase to 1.5 °C (...)" (UNFCCC, 2015). The GWLs were calculated as anomalies in the yearly global mean surface air temperature (*tas*) to the pre-industrial reference period 1850–1900 (Hauser et al., 2022; Seneviratne et al., 2021). GWLs refer to a 20-year period centered around the first year, in which the warming level is exceeded (*tas* > GWL). The methodology is based on Hauser et al. (2022), which was used for the Sixth Assessment Report of the Intergovernmental Panel on Climate Change (IPCC). We adopted the code for the use in the CanESM2-LE. To this end, we pooled all 50 members before calculating the anomalies to 1850–1900.

Our reference period 2001–2020 translates to GWL= +1.2 °C (GWL1.2) in CanESM2-LE (observed approximately 1 °C; Gulev et al., 2021). This is less an effect of the forcing scenario for RCP8.5 was shown to be in high agreement with observed emissions (Schwalm et al., 2020). Instead, it mirrors the model's rather high equilibrium climate sensitivity (3.7 K; Swart et al., 2019). Comparing modeled global *tas* with observational global mean temperature though may result in an overestimation partly due to insufficient observational data coverage and blending air temperature over land with sea surface temperatures over ocean areas in observations (Richardson et al., 2016; Vogel et al., 2019).

Future periods in our study are represented by 20-year slices centered at GWL= +2 °C (GWL2, Paris Agreement; UNFCCC, 2015) and GWL= +3 °C (GWL3, close to the most realistic end-of-century temperature of 2.8 °C under current trends in climate policy; Liu & Raftery, 2021).

Time periods corresponding to a given GWL were calculated within the global SMILE, and adopted for use in the regional SMILE.

2.3 Definition and Bivariate Evaluation of Compound Events

2.3.1 Event Definition

This study takes a multivariate perspective on dry and hot extremes, since we are particularly interested in the combined occurrences of these hazards. We employed thus the "AND" hazard scenario to connect both univariate extremes (Zscheischler & Fischer, 2020): the temporal co-occurrence of linearly detrended summer mean temperatures and (negative) precipitation sums exceeding the respective 95th percentile of 2001–2020 (with the 95th percentile of negative precipitation equaling the 5th percentile; see Supplementary figure S1). By definition, these events are expected to be very rare because both variables have to exceed a high threshold. However, since JJA temperature and negative precipitation show strong correlations in most parts of Europe, which intensified during the 21st century, CDHE occur more often than would be implied by independence (Zscheischler & Seneviratne, 2017). This implies that warm summers are commonly dry and wet summers are cool (see also Trenberth & Shea, 2005; Wang et al., 2021). Due to the extensive large ensemble database, 1000 years instead of 20 years (see fig. 1 (a)) are available per analysis period and allow for robust baseline definition (i.e., percentile estimates across all 50 ensemble members) and event characteristic estimation (e.g., frequency changes, associated behavior).

In order to characterize CDHE summer energy partitioning compared to non-CDHE summers, we employed the Bowen Ratio (BR, Bowen, 1926). The BR describes the ratio of sensible heat flux and latent heat flux, which are negatively coupled (e.g., Schwing-

shackl et al., 2017). For this analysis, we used the model variables surface upward latent heat flux and surface upward sensible heat flux.

2.3.2 Estimation of Bivariate Return Periods

In order to estimate the joint extremeness of CDHEs, we calculated bivariate return periods. Generally, return periods are the inverse of the (annual) exceedance probability p of a given event intensity, the return level z_p. Hence, the return level z_p is expected to be exceeded every $1/p$ years, defining thus the return period $T = 1/p$ (Coles, 2001). Bivariate return periods however remain ambiguous and become larger than their univariate component return periods due to the second variable that is required to meet the extremes condition as well (AghaKouchak et al., 2014; Zscheischler & Fischer, 2020). In large samples like the CRCM5-LE, (annual) event occurrences per time period can be counted and inverted to obtain the return period (Zscheischler & Fischer, 2020). This empirical approach is generally limited by the time series length. With 1000 years available, 10 events with $T = 100$ are to be expected statistically, while the most extreme case would be $T = 1000$. Any inference on this level would be highly uncertain since it is based on a single event (e.g., Zscheischler & Fischer, 2020). For shorter time series, the maximum empirical T also decreases such that extreme event estimation suffers from high uncertainties (Bevacqua et al., 2017). Instead of event counting, we here fitted copulas, i.e., multivariate probability distributions, to the bivariate distributions (Zscheischler & Fischer, 2020). The large advantage of distribution fitting is the option for pushing the rareness boundaries of the empirical approach.

For the procedure in this study we used the R package *VineCopula* (Nagler et al., 2023). First, we transformed the empirical marginals of summer temperature and precipitation (multiplied with -1 for calculation purposes) to uniform distributions on [0,1]. Next, the most suitable copula family was estimated using the Bayesian Information Criterion (BIC) and fitted to the data. For this study, we chose the locally best fitting copula family from eight single-parametric copula families (fig. S3).

Following the relation in Brunner et al. (2016), the return period T was obtained by:

$$T(u, v) = \frac{\mu}{1 - u - v + C(u, v)} \tag{1}$$

giving the probability for jointly exceeding the event defining thresholds in the denominator, with u, v corresponding to univariate probabilities of exceeding the respective threshold, $C(u, v)$ being the copula at (u, v), and the mean interarrival time $\mu = 1$ in our case since we investigated annual events (Zscheischler & Fischer, 2020; Zscheischler & Seneviratne, 2017; Brunner et al., 2016).

2.3.3 Distributional Change Assessments

Both changes in temperature and precipitation may lead to frequency changes by shifting the bivariate distribution compared to the reference period. Additionally, the bivariate (tail) dependence structure may change over time.

In order to address the first point, we here propose a method to disentangle the dominating drivers of frequency changes. Horizontal shifts of the distribution (along the orange line in fig. 1 (b)) indicate temperature changes as sole drivers whereas vertical shifts (along the blue line in fig. 1 (b)) point to precipitation changes. Any change with both a horizontal and vertical component thus is due to a combination of temperature and precipitation changes. For the definition of the dominating driver, we used the average JJA drying per degree warming (fig. 1 (b)): In Europe, the slope of this relation-

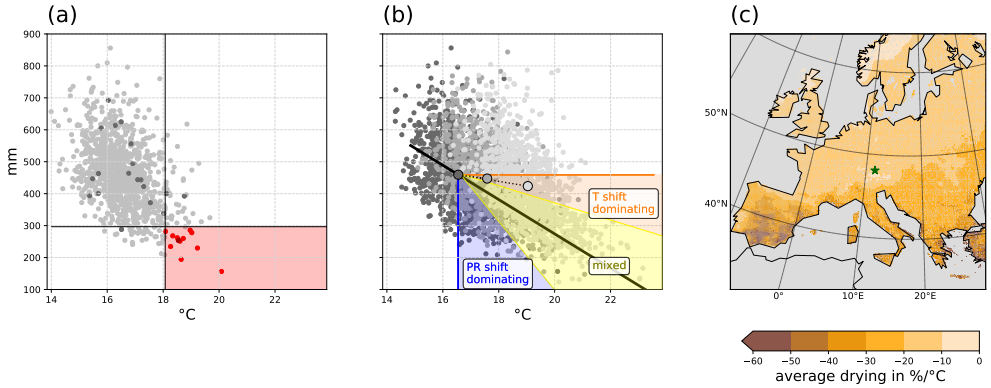

Figure 1. (a) Precipitation and temperature of 1000 summers (50 members for 2001–2020) over a grid cell representing Munich/Germany (star in (c)). Dark grey and dark red dots show the limited sample of one arbitrary member. Black lines indicate the 95th percentile of temperature (vertical) and 5th percentile of precipitation (i.e., the 95th percentile of negative precipitation; horizontal) with the red area highlighting all summers meeting the definition criterion for a CDHE. (b) Definition of temperature (orange) and precipitation (blue) dominance in distributional shifts under climate change conditions. Yellow indicates mixed contributions of temperature and precipitation (see text). Grey shaded point clouds correspond to current, GWL2, and GWL3 climates for the same pixel as in (a). The black line represents the local average summer drying scaled with warming. (c) Average summer drying scaled with warming expressed as slopes of a linear line fitted to the local bivariate distribution.

ship follows a North–South gradient with highest values in the Mediterranean area and especially over the Iberian Peninsula where summer precipitation is very low (fig. 1 (c)). Distributional shifts along this slope represent the occurrence of more extreme events by heating and drying following the current relationship. If the center of the distribution is shifted within the orange sector of fig. 1 (b), temperature is identified as dominating driver, while it is precipitation for shifts into the blue sector. Since we are also interested in simultaneous changes of temperature and precipitation, we introduced a buffer zone between a line with half the local slope and a line with twice the local slope to account for uncertainties in slope estimation (yellow sector). This combination is further referred to as mixed drivers. This approach is based on correlation of the full distributions, which, as Zscheischler and Seneviratne (2017) argue, can serve as an indicator for the likelihood of CDHE if the percentile threshold for event definition is not too high.

To account for dependencies in the distribution extremes, tail (= extremal) dependence above the 95th univariate percentiles (chi(0.95); Coles et al., 1999) were calculated for each period separately using the R package *extRemes* (Gilleland, 2022). Confidence intervals at the 0.05 level were obtained by bootstrapping 1000 times.

2.4 Assessment of CDHE Impacts on Soil Moisture

In one of the first compound event definitions by Leonard et al. (2014), compound events are defined by the extremeness of impacts originating from multiple contributing hazards. While our CDHE definition rather follows a hazard-based perspective, we nevertheless aim to assess CDHE effects in this study. Our (univariate) target variable is soil moisture, classified as the soil moisture index (SMI) of Zink et al. (2016), which also forms the basis of the German Drought Monitor. The SMI is based on soil mois-

ture percentiles of a reference period (2001–2020 in our case). We used JJA soil moisture in the upper portion of the soil column to assess agricultural droughts during current climate, GWL2, and GWL3. Soil moisture is especially useful when assessing event impacts, for soil moisture droughts have large agricultural and ecosystem-specific impacts. Assessing soil moisture conditions is hence most relevant in areas where they potentially have an impact. Therefore, we confined our analyses of CDHE–soil moisture relationships on European agricultural areas. These comprise Corine Land Cover (CLC2018 version 2020_20u1, linearly regridded to CRCM5-LE spatial resolution; EEA, 2020) level-2 classes *arable land*, *permanent crops*, and *heterogeneous agricultural areas*.

3 Results

3.1 Bowen Ratio Increases During CDHE

CDHE and non-CDHE summers differ with respect to the energy-partitioning of sensible and latent heat flux. In order to illustrate these differences in a spatially explicit way, we first look at the Bowen Ratio during summer under current climate conditions. During non-CDHE summers, the latent heat flux, i.e., evaporative cooling (O et al., 2022), is dominating over the sensible heat flux in large areas of Europe (fig. 2 (a)–(b)). These coincide with the wet evapotranspiration regions (energy-limited) of Schwingshackl et al. (2017). The dominating low BR conditions favor widespread cloud formation and summer precipitation. In CDHE summers (fig. 2 (b)), however, BR increases in large areas. High BR occurs in their wet/transition regions (moisture-limited). Zscheischler et al. (2015) state that under dry conditions, evapotranspiration and temperature are strongly dominated by soil moisture. Especially the Mediterranean regions, the lower course of the Danube and coastal regions of the Black Sea experience BR > 10. Under these conditions, a reduced latent heat flux (and hence evaporation) suggests low soil moisture availability, while temperatures rise (Mukherjee et al., 2023). Consequently, cloud convection and precipitation are inhibited.

We find no BR inversions or only small increases during CDHE in Northern and central Europe as well as in mountainous regions (fig. 2 (a)–(b)). However, these regions are characterized by evaporation increases (and hence soil drying) during CDHE summers (fig. 2 (c)). This suggests an increase in latent heat flux and, potentially, a reduced temperature increase due to evaporative cooling (O et al., 2022). These regions are characterized by an energy-limited evapotranspiration regime (Teuling et al., 2009), where higher temperatures in CDHE summers compared to non-CDHE summers favor evaporation. The remainder of the domain, largely defined by soil-moisture limited evapotranspiration regimes (Teuling et al., 2009), experiences major evaporation reductions (fig. 2 (c)), presumably due to moisture limitations in comparison to non-CDHE summers. High BR values, i.e., low latent heat flux compared to sensible heat flux, may result from low soil moisture conditions (Trenberth & Shea, 2005). Since soil moisture and evaporation mutually influence each other and CDHE affect evaporation (Miralles et al., 2019), we conclude here that soil moisture is affected by CDHE occurrences as well.

The described relationships for CDHE and non-CDHE hold true for GWL2 and GWL3 (see supplementary fig. S2 for BR evolution under GWL2 and GWL3).

3.2 CDHE Frequency Increases

CDHE occur rarely under current climate conditions (fig. 3 (a)). Assuming no dependence between temperature and precipitation, the occurrence probability of a CDHE would amount to $0.05 \times 0.05 = 0.0025 = 0.25$ events per 100 years. This corresponds to a 1-in-400 year event. This very rare frequency is however exceeded over most of Europe. Assuming total dependence, the frequency has an upper limit at 5 events per 100 years by definition of the CDHE events, equaling a 1-in-20 year event. In the CRCM5-

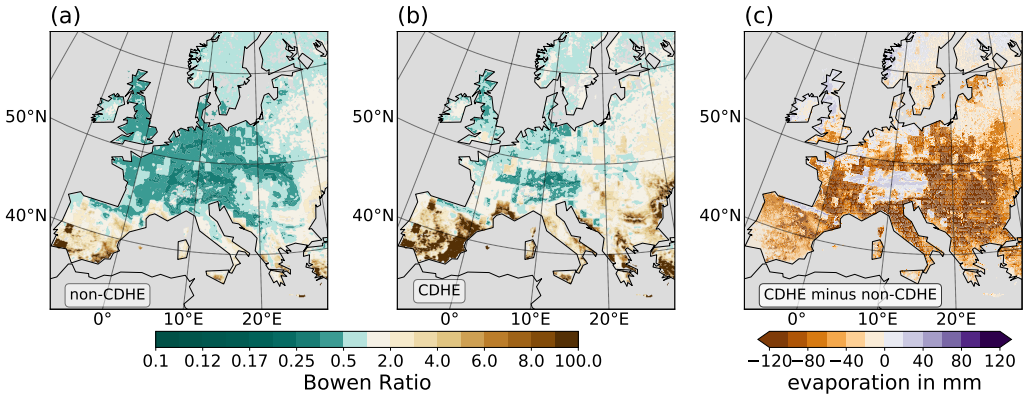

Figure 2. Bowen Ratio for non-CDHE summers (a) and CDHE summers (b) under current climate conditions. The median across all ensemble members is shown per category. Brownish colors indicate regions with sensible heat > latent heat, greenish colors indicate regions with sensible heat < latent heat. (c) evaporation increases (purple) and decreases (orange) in CDHE summers compared to non-CDHE summers under current conditions.

LE, highest event frequencies reach 3.5 events per 100 years in central eastern Europe (roughly 1-in-28 year event). On the contrary, parts of the Mediterranean, Aegean and Black Sea coastal regions as well as Southern Ireland, Northern France, and mountainous regions in central and Northern Europe encounter $<$ 0.5 events per 100 years which corresponds to a 1-in-200 year event.

For GWL2, event frequencies regionally double to triple, with strongest increases in Southern Europe and weakest changes in Northern and central eastern Europe as well as the Western Iberian Peninsula (fig. 3 (b)). No decreases are detected. Interestingly, while some regions with highest event frequencies under current conditions, e.g., central eastern Europe, encounter only increases by $<$ 3 events per 100 years, Southeastern France both shows high frequencies under current conditions and strong increases under GWL2. Contrasting to that, the coastal areas of the Mediterranean, Aegean and Black Sea with low event occurrences under current conditions experience an even higher increase by 6–9 events per 100 years.

With further ascending GWL, event frequencies surge (fig. 3 (c)): Especially in mountainous forelands of Northern/Northeastern Spain and central/Southwestern France more than 1 out of 4 years under GWL3 qualify as a CDHE with respect to current percentile definitions (adding frequencies in fig. 3 (a) and (c)). The same holds true for the Po Valley in Northern Italy. Regions north of the Alps, in Northern France, Southern Ireland or the Western Iberian Peninsula with currently very few events ($<$ 0.5 per 100 years) experience up to $>$ 15 events per 100 years in addition to current frequencies. Eastern Europe and the Balkans are characterized by a North–South gradient of increases. Lowest gains are found in Scandinavia, Northeastern Europe, the highest Alpine ridges, and Southern Spain. To put these numbers into perspective, Toreti et al. (2019) show that 2018-like droughts mirror typical summer conditions by the 2040s, using a multi-model ensemble under RCP8.5.

3.3 Drivers of CDHE Frequency Increases

What is driving these frequency increases? In fig. 4, we investigate changes in the bivariate distribution of temperature and precipitation. First, fig. 4 (a)–(b) demonstrate the prevalent dominance of temperature increases in shifting the distribution into the

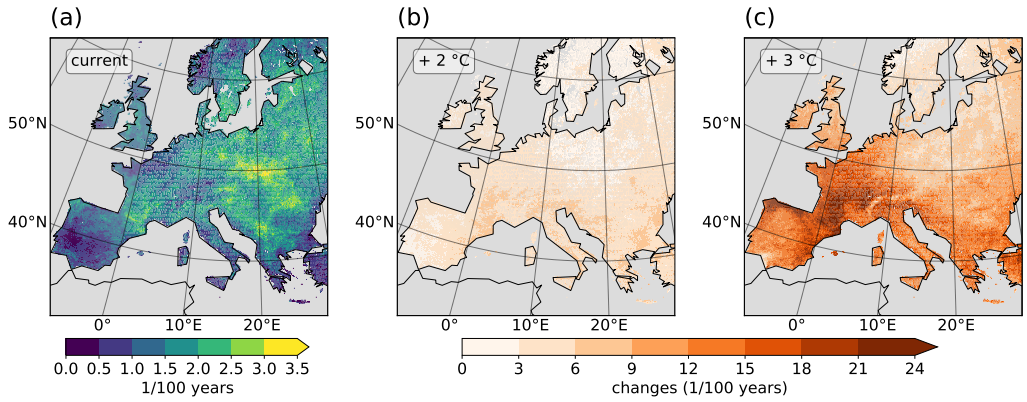

Figure 3. CDHE frequency for three global warming levels (absolute values for present climate (a) and changes under GWL2 (b) and GWL3 (c)). Events are defined as local exceedance of the current (2001–2020) 95th percentile of temperature and (negative) precipitation.

defined CDHE diagram space (see also fig. 1 (b)) under both GWL2 and GWL3. Precipitation dominates in mountainous Norway and Northern Spain. In the Atlantic regions of Western Europe, temperature and precipitation changes jointly foster frequency increases. Under GWL3 conditions, these areas with mixed drivers expand towards the East. In addition, precipitation dominance emerges from previously mixed driver regions. This finding mirrors earlier emergence of (mean summer) temperature trends compared to higher uncertainty and variability in precipitation trends (e.g., von Trentini et al., 2019; Seneviratne et al., 2021). For large parts of Europe, precipitation variability defines hence whether a CDHE occurs, if (nearly) every year exceeds the present temperature threshold of event definition (consistent with e.g., Zscheischler & Fischer, 2020).

Secondly, we consider the dependence structure of the distributions (fig. 4 (c)–(e)). As stated above, a tail dependence of 1 implies that each temperature extreme (as defined here) is associated with a precipitation extreme and vice versa. The joint occurrence probability of CDHE is thus 0.05 (i.e., 5 events per 100 years) and hence the same as for univariate extremes in our definition. On the contrary, a tail dependence of 0 implies independent behavior of temperature and precipitation extremes and thus a probability of $0.05 \times 0.05 = 0.0025$ (i.e., 0.25 events per 100 years in our case). It follows that the spatial distribution in fig. 4 (c) mirrors the spatially distributed CDHE frequencies (fig. 3 (a)) with highest tail dependence corresponding to highest event frequencies in central eastern Europe and bivariate tail independence in mountainous Norway, Northern France, Southern Ireland, inner Alpine regions, and Mediterranean coastal regions with very rare CDHE occurrence. Under GWL2, the tail dependence exceeds the current 95 % confidence interval especially in regions with currently low tail dependence values (e.g., Northeastern France and Northern Italy, the Danube delta or mountainous Norway, fig. 4 (d)). In these regions, the tail dependence increase may add to event frequency. Tail dependence reductions are found on the western Iberian Peninsula with already low values and, notably, in central eastern Europe with currently highest values. More spatially distinct clusters emerge under GWL3 (fig. 4 (e)), where robust tail dependence increases occur in Northern France, Southern UK and Ireland, the Alpine (foreland) and Cantabrian Mountain regions, and Scandinavia. Tail dependence decreases, e.g., in Southern Sweden, parts of the Iberian Peninsula, and central eastern Europe. In South-western Spain, this decrease may contribute to the rather low CDHE occurrence increase under GWL3 conditions (see fig. 3 (c)). Tail dependence changes are reflected by changes in the underlying copula family (supplementary fig. S3 (a)–(c)): For example, tail depen-

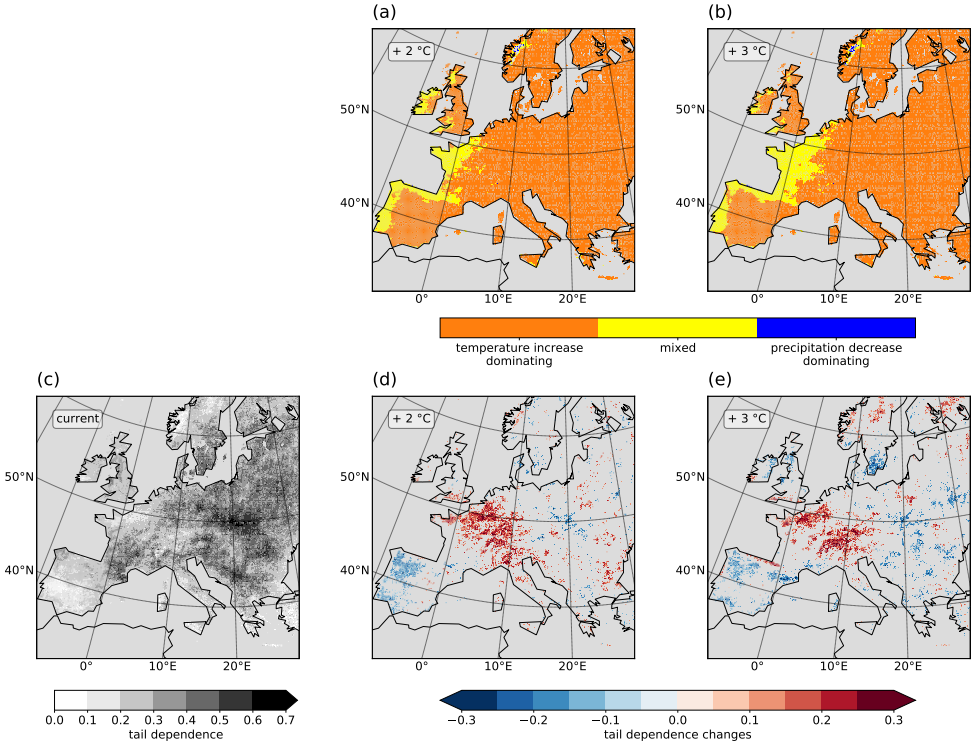

Figure 4. Changes in combined temperature and precipitation distributions. (a)–(b) distributional shifts due to temperature increases (orange), precipitation decreases (blue) or both (yellow) following the approach from fig. 1 (b)). Only land areas with significant correlations of JJA temperature and precipitation are colored. (c)–(e) tail dependence of temperature and (negative) precipitation: (c) current absolute values, changes for GWL2 (d) and GWL3 (e). For GWL2 and GWL3 only regions with changes exceeding the present 95 % confidence interval are shown. Note: The tail dependence refers to the tails above the respective 95th temperature and (negative) precipitation percentile of each period.

dence increases mostly correspond to switches from symmetric copula families (mostly Gaussian or Frank) to asymmetric families (e.g., Gumbel which only occur in regions with BR $<$ 1 under current conditions). Decreases are associated with the inverted switch. Symmetric families represent regions with amplified tail dependence in the hot-dry and cold-wet tail, whereas asymmetric families include only one tail with enhanced dependence. Note that the bivariate structure is generally weak to moderate in most regions (theoretical Kendall's τ with $0.2 < \tau < 0.5$, fig. S2 (d)–(f)), pointing towards rather similar bivariate distributions. With increasing GWL, τ increases in Western Europe, hence strengthening the differences between the joint summer temperature–precipitation distributions.

The tail dependence also allows for a quick change of perspective: Since it is calculated with respect to each period (current, GWL2, GWL3), we are also able to infer that CDHEs defined relative to the percentiles of each period occur more (less) frequently where tail dependence increases (decreases).

3.4 Soil Moisture Scaling with CDHE Extremeness

To account for the risk that agricultural droughts, i.e., soil moisture deficits, pose on crops, we focus our further assessment on European agricultural regions.

We start our assessment with return periods T of CDHE in current, GWL2, and GWL3 conditions (fig. 5 (a)–(c)). Therefore, we ask the question: How extreme would a future CDHE be in relation to the current temperature and precipitation distribution? Since higher return periods correspond to hotter and drier summers with respect to current CDHE, they are interpreted as surrogates for joint event intensity. T is obtained for the 95th percentile of temperature and (negative) precipitation of the respective periods from the copula fitted to the present bivariate distribution. Hence under current conditions (fig. 5 (a)), the distribution again mirrors the current tail dependence (fig. 4 (c)) and event frequency distribution (fig. 3 (a)). The theoretical minimum return period of the current period is $T = 20$ (perfect tail dependence), the maximum $T = 400$ (independence). Consistent with that, we find among the CDHE just passing both thresholds return periods of $T = 30$ to $T = 300$ in the current period. Under GWL2 conditions (fig. 5 (b)), return periods increase to several hundreds to thousands of years with respect to the current distribution. In single grid cells (dark red), the extremeness of these CDHE is unprecedented ($T = \text{inf.}$). In these cases, (mostly) future temperature or precipitation lie outside the margins of the current distribution. Hence CDHE of this extremeness did not occur at all in the current period of the CRCM5-LE. Under GWL3 (fig. 5 (c)), these CDHE are dominating across Europe: We find $T = 1000$ to $T = 3000$ years in eastern Germany, Poland, and the Baltics, whereas the remainder of Europe is subject to CDHE with a current occurrence probability $p = 0$. To generalize, the conditions of CDHE definition correspond to highly unlikely current conditions when considering GWL2, and unprecedented conditions in GWL3.

During all summers exceeding the respective CDHE definition in current, GWL2, and GWL3 climates (fig. 5 (d)–(f)), extreme (below 5th percentile) or exceptional droughts (below 2nd percentile) prevail in European agricultural regions. Exceptions are very southerly parts (Southern Spain, Turkey) where the soil moisture content corresponds to moderate (below 20th percentile) or severe (below 10th percentile) droughts. However, since SMI classes are calculated with respect to the local distribution and the local distributions do not always range from total depletion to total saturation, the 'less severe' categories may represent low absolute soil moisture conditions as well, while more severe drought conditions in humid regions may represent higher absolute soil moisture conditions. With rising GWL, virtually all European agricultural areas experience exceptional drought conditions during future CDHE.

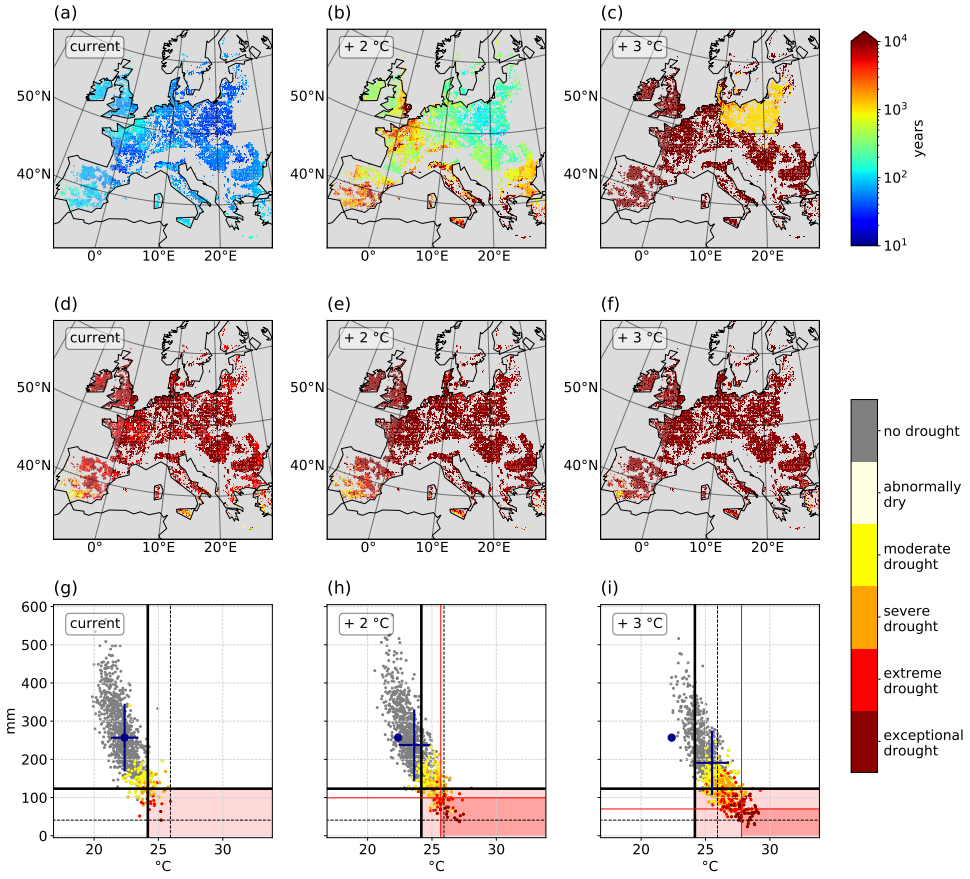

Figure 5. CDHE intensity for current, GWL2 and GWL3 conditions in European agricultural regions. (a)–(c) return period of summers with temperatures and (negative) precipitation at the GWL-specific 95th percentile (crosses of thick black lines in (g) and red lines in (h) and (i). (d)–(f) average SMI categories during all summers exceeding the GWL-specific 95th percentiles of temperature and (negative) precipitation. (g)–(i) scatter plots of summer precipitation against summer temperature for an example region (Po Valley, Northern Italy). Thick (thin) black lines show the present 5th and 95th percentiles (minimum and maximum) for precipitation and temperature, respectively. Red lines mark the 5th and 95th percentiles for GWL2 and GWL3. Light red background highlights current CDHE summers; strong red background CDHE summers for GWL2 and GWL3 percentiles. Blue dots show the current mean, crosses span one standard deviation of the respective periods for temperature and precipitation. Colors in (d)–(i) indicate soil moisture drought categories (percentiles) with respect to the current period following Zink et al. (2016).

Figures 5 (g)–(i) further show the relationship among soil moisture droughts and compound events in an example region (Po Valley, south of the Alps) to illustrate the relationship between temperature, precipitation and SMI in all summers: Summers within the shaded diagram space (i.e., CDHE) are affected by more extreme SMI categories in all periods; under GWL3 the majority of CDHE summers corresponds to 'exceptional drought' (fig. 5 (i)). Soil moisture drought extremeness follows the distributional axis, (i.e., not dominantly along the temperature or precipitation axis). With progressing global climate change, distribution shifts towards warmer and drier conditions (see crosses relative to blue dots in (h) and (i)) increase the frequency of summers within the light red shaded diagram space and also more extreme SMI. The majority of CDHE summers in GWL2 and GWL3 is characterized by unprecedented temperatures (dotted black vertical line) and numerous future events undercut the driest current summer as well (dotted black horizontal line). This fact illustrates why this region is colored in dark red in fig. 5(c). CDHE frequencies even increase with respect to the future percentiles (dark red shaded diagram space) which aligns with risen tail dependence in this region (fig. 4 (h)–(i)). Overall, figs. 5 (g)–(i) suggest a stable relationship of high (low) absolute temperature (precipitation) values and soil moisture drought categories.

Last, how is bivariate extremeness of summers related to SMI? Figures 6 (a)–(c) provide Spearman rank correlations well below -0.8 in most of European agricultural areas. This strong relationship implies that more extreme CDHE translate to lower moisture conditions. Note that the correlation does not allow to conclude whether CDHE are triggered or enhanced by low SMI values or vice versa, e.g., via land-atmosphere feedbacks. As discussed in Manning et al. (2019) and Mukherjee et al. (2023), both is plausible and most likely interconnected. In addition, soil moisture effects from previous seasons or years (Felsche et al., 2023; Bastos et al., 2020) may confound the effect of CDHE on soil moisture conditions of the same summer. The correlation is highly linear in all GWLs (fig. 6 (d)–(f)), with a shift from low event extremeness and high soil moisture in the example region during current conditions to high event extremeness and low soil moisture conditions under GWL3. Again, this mirrors large projected CDHE frequency increases both in absolute terms and relative to all summers of a given GWL epoch. These summers hence pose a triple hazard to ecosystems and agriculture in the affected regions, arising from low soil moisture, high temperature and thus high water demand for transpiration, and low precipitation.

4 Discussion

In this study, we assessed frequency increases of European CDHE within a regional SMILE, drivers of these increases, and the association of CDHE with soil moisture droughts. The study does not provide insights in the causal directions of the SMI–CDHE relationship, i.e., answer the question whether low soil moisture results in or from CDHE occurrence.

Defining CDHE based on summer precipitation percentiles comes at a cost as we found in our results: In very dry regions, precipitation fluctuates on a low level. Hence, due to the local JJA precipitation distribution, absolute differences between years below or above the percentile threshold are rather small. Here, temperature variability defines whether a CDHE occurs during a given period. Note that this is a different effect than precipitation variability driving CDHE occurrence in areas where regional warming induces yearly exceedance of the temperature threshold. Compared to the remainder of the domain, lag effects may play a more important role in soil moisture contents in areas with very low JJA precipitation sums. In general, CDHE may be more precisely defined with a Survival Kendall hazard definition instead of the AND definition (see, e.g., in fig. 5 (g)–(i), Salvadori et al., 2016). However, the correlation of SMI and CDHE extremeness is highly linear even in our simplified event definition.

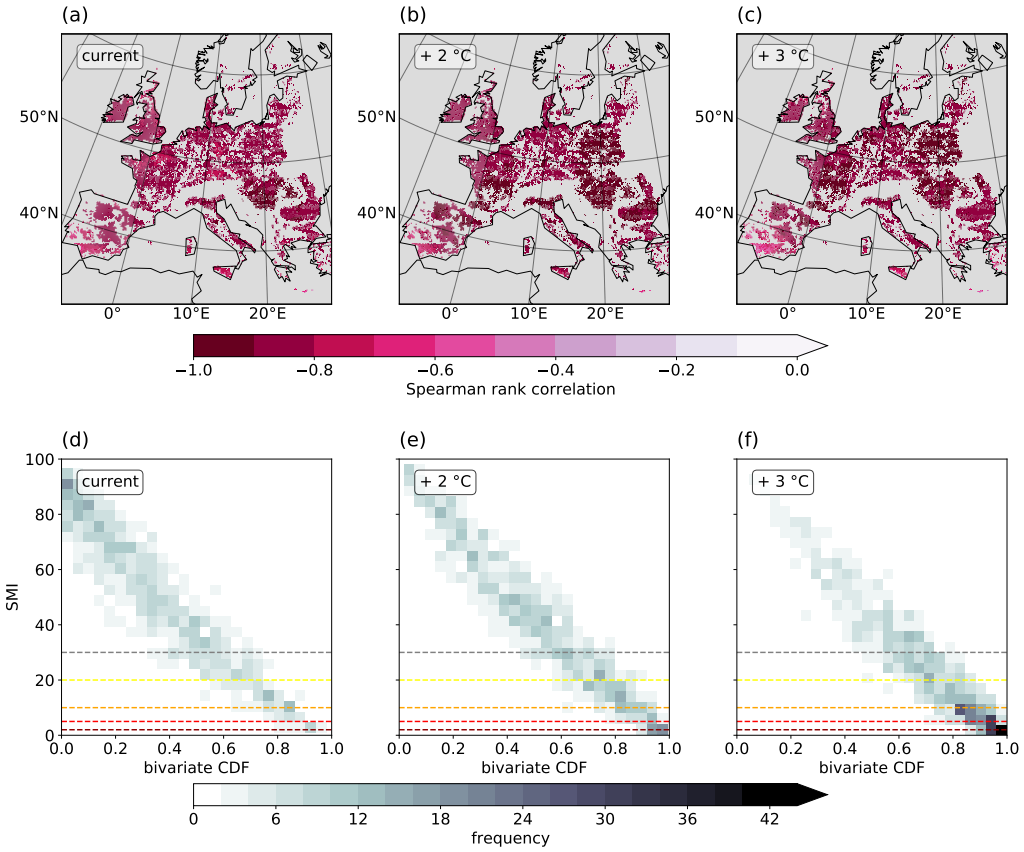

Figure 6. Relationship between CDHE extremeness (relative to conditions of the current period) and SMI values. (a)–(c) Spatially distributed Spearman rank correlation of CDHE extremeness and SMI values. (d)–(f) bivariate histograms of spatially aggregated CDHE extremeness and SMI in an example region (Po Valley, Northern Italy). Colors indicate the amount of summers in a given square. Dashed lines correspond to abnormally dry (grey), moderate drought (yellow), severe drought (orange), extreme drought (red), and exceptional drought (dark red) SMI conditions expressed as percentiles following Zink et al. (2016).

For explaining CDHE frequency increases, we focused on temperature and precipitation mean shifts, i.e., no variability or higher-order distributional changes which are represented, e.g., in the marginal changes in François and Vrac (2023). Inspections of local distributions showed that for summer CDHE variability changes only marginally under GWL2 and GWL3 (e.g., fig. 5 (d)–(f)). Shifts of the joint distributions alone were shown to considerably increase CDHE frequencies – not only in arid regions as done by Hao et al. (2018) and Mukherjee and Mishra (2021), but also in transitional/humid regions. Our approach is limited by the margins of the current temperature and precipitation distributions since we relate future events to the current distribution. Nevertheless, we showed that the joint increase of hot and dry extremeness can be used as a qualitative intensity measure. Beyond that, Wang et al. (2021) pointed to regionally intensifying negative correlations between temperature and precipitation over the last decades which led to an increase of CDHE, especially in the form of more heat events during droughts. However, we show that not only correlation of the full distribution is projected to change with rising GWL, but also the distributional tails and the entire dependence structure. Bivariate dependence structures in models though require cautious consideration. Zscheischler and Fischer (2020) point towards an underestimation of temperature and precipitation tail dependence in CMIP5 models. This would imply a potential underestimation of CDHE. A more detailed investigation into bivariate distributional characteristics in model and observational data is hence advisable for locally specific assessments.

By reaching GWL3 in the middle of the 21st century (2042–2061) under RCP8.5, the CanESM2 driving the CRCM5-LE proves to be a rather hot global climate model. We therefore used a relative model- and scenario-independent measure of time, i.e., the GWL, to overcome the effect of an intrinsically 'hot' global climate model with a high-emission scenario. Assessing uncertainties related to this approach requires comparative studies in other model SMILEs and with other scenarios. Yet, so far, there is only a very limited number of regional SMILEs (typically with only few members) available (e.g., Aalbers et al., 2018).

As argued in Jha et al. (2023), the selection of warming levels and models explains most of the uncertainty in CDHE changes over Europe. The choice of copula families contributes the least in their assessment, while Zscheischler and Fischer (2020) argue that event definition and copula fitting affect the final probability and therefore extremeness of events. In our study, we attempted to reduce this kind of uncertainty by not focusing on single events. Instead, the SMILE served as a basis for investigating general characteristics of a large number of events, thus reducing the influence of outliers. Testing several copula families helped to find the locally best fitting bivariate distribution. Further, while in principle the SMILE provides the required size to sample low-probability events ($T = 1000$), we found that future events tend to be clearly more rare than current 1-in-1000 year events. Hence, even the large ensemble is insufficient for empirical estimations and distributional sampling is necessary.

Using the SMILE though allows for a robust sampling of internal variability which potentially masks dependence changes in setups with few members (Bevacqua et al., 2023). In addition, differing states of large-scale atmospheric modes prevalent in single members during the selected period of investigation may trigger differences in compound event frequencies (Bevacqua et al., 2023). This shows the high importance of internal variability in the evaluation of low-probability events and justifies the use of a SMILE.

While the CRCM5-LE provides high geographical detail in the spatial distribution of frequency (changes), results are affected by coarse resolution geophysical inputs as is visible in fig. 2: The tiling pattern resolution (1°) is coarser than the CRCM5 resolution, but finer than the spatial resolution of the driving general circulation model CanESM2. In central Europe, high bedrock depths (i.e., large soil column) coincide particularly well with low BR in fig. 2 (b) and high evaporation in fig. 2 (c). Presumably, a large soil column contributes more strongly to evaporation than neighboring areas with thin soil columns.

However, this assumption requires further investigation, as well as implications on the reliability of other variables. For instance, this effect is also visible in the upper distributional tail of temperature at high temporal resolution (see also Miller et al., 2023). In spite of this, the regional SMILE allowed to highlight hotspots of event frequency (changes) and regionally varying driver dominance in high geographical detail. This is a large advantage of our study over similar analyses with coarse-resolution global SMILEs: For example, a distinction of coastal or mountainous regions would not be possible on a coarse grid since the small-scale features cannot be resolved. Hence, the derivation of relevant drivers or dependence changes would have been impeded.

Given considerable frequency increases of CDHE and their association to low soil moisture contents, we argue that the relationship between both deserves further investigation. Denissen et al. (2022) show that soil moisture limited conditions represent the new normal under a high-emission global warming scenario in that they intensify and expand in length. Since it has been shown that heatwaves, droughts or compound CDHE can be triggered by depleted soils (Fischer et al., 2007), investigating CDHE effects on soil moisture is also crucial in bringing forth the research on potential legacy effects on subsequent seasons or years (e.g., CDHE triggering subsequent CDHE mediated by prevailing soil depletion). CDHE may exert influence not only on temporally, but also spatially distant events: Li et al. (2023) show that dry soils in upwind regions may lead to propagation of events and, adding onto local land-atmosphere coupling, affect crop yields downwind of events. For example, these authors found that maize failure in Southeastern Europe and wheat failure in Italy tend to be associated with dry and hot conditions.

5 Conclusions

We find that European compound hot and dry summers are characterized by an increase of evaporative demand in the atmosphere, but with reduced evaporation in most regions, presumably due to soil moisture deficits. Mountainous regions experience increased evaporation, most likely due to higher temperatures and still dominant energy limitation of their evaporation regime. The frequency of CDHE summers increases considerably in Europe under climate change conditions. Owing to the high spatial resolution of our SMILE, we robustly identify regions in Southern France and Northern Spain as hotspots due to highest absolute increases, whereas, e.g., Southern Germany, Northern France, Southern Ireland, or the southwestern Black Sea coast can be identified as currently low-frequency areas with highest multiplication of events under climate change. Apart from Western European regions, Northern Spain and mountainous Norway, frequency increases can be mostly attributed to rising temperatures. Yet, climate change also affects the bivariate dependence structure of temperature and precipitation, fostering tail dependencies and hence the co-occurrence of dry and hot conditions. Further, events intensify with respect to the current conditions of precipitation and temperature. Soil moisture during CDHE is projected to remain extremely low under GWL2 and GWL3 in agricultural regions and shows particularly strong negative correlations with bivariate summer intensity.

This study finds newly emerging CDHE hotspots in European areas with yet unseen combinations of extremely hot and dry conditions. Regardless of the causal directions in the SMI–CDHE relationship, the tight relationship of low soil moisture and CDHE therefore poses an increasing risk to agriculture that requires consideration in adaptation planning.

This study also shows an ordering of temperature and precipitation changes in driving the frequency increases: For GWL2, temperature increase is the major driver of CDHE frequency increases. For GWL3, precipitation decrease additionally emerge as important driver (in the form of mixed contributions). Here, it would be interesting to further investigate the processes and mechanisms driving local dependence increases or decreases.

The regional SMILE is particularly apt for analyzing compound events in the extreme tails of the bivariate distribution. Climate change is shown to produce events that are much rarer than any observed summer, while currently extremely rare events become the new normal. Fitting distributions instead of counting the summers that meet the event definition criteria hence allows to avoid a saturation effect related to the maximum empirical event rareness under current conditions (i.e., $T = 1000$ years). Using SMILEs, further research can elucidate potential benefits of increasing sample sizes in reducing the uncertainty ranges of distribution fitting for extremely rare events.

Last, we conclude that limiting global warming to +2 °C considerably reduces CDHE hazards in Europe, which regionally then results in half the amount of summers with extremely low soil moisture availability. Since the risk of impacts on human systems depends on resilience structures in the affected regions (e.g., Lesk et al., 2016), hazard reduction should be accompanied by fostering resilience towards CDHE effects as well.

Open Research Section

The CRCM5-LE data used for all performed analyses is described in Leduc et al. (2019) and available at https://www.climex-project.org/en/data-access/

Corine land cover data is provided by the European Union, Copernicus Land Monitoring Service 2018, European Environment Agency (EEA) at https://land.copernicus.eu/pan-european/corine-land-cover

Codes to perform the presented analyses and obtain the figures will be shared through a public repository upon publication of the manuscript.

Acknowledgments

This research was conducted within the ClimEx project (www.climex-project.org) funded by the Bavarian State Ministry for the Environment and Consumer Protection (Grant No. 81-0270-024570/2015). CRCM5 was developed by the ESCER Centre of Université du Québec à Montréal (UQAM; https://escer.uqam.ca/, last access: 14 June 2023) in collaboration with Environment and Climate Change Canada. Computations with the CRCM5 for the ClimEx project were performed on the HPC system SuperMUC and the Linux Cluster of the Leibniz Supercomputing Center LRZ, Bavarian Academy of Sciences and the Humanities (BAdW), funded via GCS by BMBF and StMWFK. The authors gratefully acknowledge the Leibniz Supercomputing center for funding this project by providing computing time on its Linux-Cluster. Further, the authors would like to thank H. Funk for fruitful discussions on copula use.

References

Aalbers, E. E., Lenderink, G., van Meijgaard, E., & van den Hurk, B. J. J. M. (2018). Local-scale changes in mean and heavy precipitation in western europe, climate change or internal variability? *Climate Dynamics*, *50*, 4745-4766. Retrieved from `https://doi.org/10.1007/s00382-017-3901-9` doi: 10.1007/s00382-017-3901-9

Afroz, M., Chen, G., & Anandhi, A. (2023). Drought- and heatwave-associated compound extremes: A review of hotspots, variables, parameters, drivers, impacts, and analysis frameworks. *Frontiers in Earth Science*, *10*. Retrieved from `https://www.frontiersin.org/articles/10.3389/feart.2022.914437` doi: 10.3389/feart.2022.914437

AghaKouchak, A., Cheng, L., Mazdiyasni, O., & Farahmand, A. (2014). Global warming and changes in risk of concurrent climate extremes: Insights from the 2014 california drought. *Geophysical Research Letters*, *41*(24), 8847-8852. Retrieved from `https://agupubs.onlinelibrary.wiley.com/doi/abs/`

10.1002/2014GL062308 doi: https://doi.org/10.1002/2014GL062308

Bastos, A., Ciais, P., Friedlingstein, P., Sitch, S., Pongratz, J., Fan, L., ... Zaehle, S. (2020). Direct and seasonal legacy effects of the 2018 heat wave and drought on european ecosystem productivity. *Science Advances*, *6*(24), eaba2724. Retrieved from https://www.science.org/doi/abs/10.1126/sciadv.aba2724 doi: 10.1126/sciadv.aba2724

Bevacqua, E., Maraun, D., Hobæk Haff, I., Widmann, M., & Vrac, M. (2017). Multivariate statistical modelling of compound events via pair-copula constructions: analysis of floods in ravenna (italy). *Hydrology and Earth System Sciences*, *21*(6), 2701–2723. Retrieved from https://hess.copernicus.org/articles/21/2701/2017/ doi: 10.5194/hess-21-2701-2017

Bevacqua, E., Suarez-Gutierrez, L., Jézéquel, A., Lehner, F., Vrac, M., Yiou, P., & Zscheischler, J. (2023). Advancing research on compound weather and climate events via large ensemble model simulations. *Nature Communications*, *14*, 2145. Retrieved from https://doi.org/10.1038/s41467-023-37847-5 doi: 10.1038/s41467-023-37847-5

Bowen, I. S. (1926). The ratio of heat losses by conduction and by evaporation from any water surface. *Physical Review*, *27*, 779-787.

Brunner, M. I., Seibert, J., & Favre, A.-C. (2016). Bivariate return periods and their importance for flood peak and volume estimation. *WIREs Water*, *3*(6), 819-833. Retrieved from https://wires.onlinelibrary.wiley.com/doi/abs/10.1002/wat2.1173 doi: https://doi.org/10.1002/wat2.1173

Buras, A., Rammig, A., & Zang, C. S. (2020). Quantifying impacts of the 2018 drought on european ecosystems in comparison to 2003. *Biogeosciences*, *17*(6), 1655–1672. Retrieved from https://bg.copernicus.org/articles/17/1655/2020/ doi: 10.5194/bg-17-1655-2020

Böhnisch, A., Felsche, E., & Ludwig, R. (2023). European heatwave tracks: using causal discovery to detect recurring pathways in a single-regional climate model large ensemble. *Environmental Research Letters*, *18*(1), 014038. Retrieved from https://dx.doi.org/10.1088/1748-9326/aca9e3 doi: 10.1088/1748-9326/aca9e3

Böhnisch, A., Mittermeier, M., Leduc, M., & Ludwig, R. (2021). Hot spots and climate trends of meteorological droughts in europe–assessing the percent of normal index in a single-model initial-condition large ensemble. *Frontiers in Water*, *3*. Retrieved from https://www.frontiersin.org/articles/10.3389/frwa.2021.716621 doi: 10.3389/frwa.2021.716621

Ciais, P., Reichstein, N., M.and Viovy, Granier, A., Ogée, J., Allard, V., Aubinet, M., ... Valentini, R. (2005). Europe-wide reduction in primary productivity caused by the heat and drought in 2003. *Nature*, *437*, 529–533. Retrieved from https://doi.org/10.1038/nature03972 doi: 10.1038/nature03972

Coles, S. (2001). *An introduction to statistical modeling of extreme values*. Springer London.

Coles, S., Heffernan, J., & Tawn, J. (1999). Dependence measures for extreme value analyses. *Extremes*, *2*, 339–365. Retrieved from https://doi.org/10.1023/A:1009963131610 doi: 10.1023/A:1009963131610

Denissen, J. M. C., Teuling, A. J., Pitman, A. J., Koirala, S., Migliavacca, M., Li, W., ... Orth, R. (2022). Widespread shift from ecosystem energy to water limitation with climate change. *Nature Climate Change*, *12*, 677–684. Retrieved from https://doi.org/10.1038/s41558-022-01403-8 doi: 10.1038/s41558-022-01403-8

EEA, E. E. A. (2020). *Corine land cover (clc) 2018, version 2020_20u1.* (https://land.copernicus.eu/pan-european/corine-land-cover/clc2018?tab=metadata. Last accessed: 9 June 2023)

Felsche, E., Böhnisch, A., & Ludwig, R. (2023). Inter-seasonal connection of typical european heatwave patterns to soil moisture. *npj Climate and Atmospheric*

Science, *6*(1), 1. doi: https://doi.org/10.1038/s41612-023-00330-5

Fischer, E. M., Seneviratne, S. I., Lüthi, D., & Schär, C. (2007). Contribution of land-atmosphere coupling to recent european summer heat waves. *Geophysical Research Letters*, *34*(6). Retrieved from https://agupubs.onlinelibrary.wiley.com/doi/abs/10.1029/2006GL029068 doi: https://doi.org/10.1029/2006GL029068

François, B., & Vrac, M. (2023). Time of emergence of compound events: contribution of univariate and dependence properties. *Natural Hazards and Earth System Sciences*, *23*(1), 21–44. Retrieved from https://nhess.copernicus.org/articles/23/21/2023/ doi: 10.5194/nhess-23-21-2023

Fyfe, J. C., Derksen, C., Mudryk, L., Flato, G. M., Santer, B. D., Swart, N. C., ... Jiao, Y. (2017). Large near-term projected snowpack loss over the western United States. *Nature Communications*, *8*. Retrieved from https://doi.org/10.1038/ncomms14996 doi: 10.1038/ncomms14996

Gilleland, E. (2022). *extremes: Extreme value analysis. r package version 2.1-3.* Retrieved from https://staff.ral.ucar.edu/ericg/extRemes/

Gulev, S., Thorne, P., Ahn, J., Dentener, F., Domingues, C., Gerland, S., ... Vose, R. (2021). Changing state of the climate system. In V. Masson-Delmotte et al. (Eds.), *Climate change 2021: The physical science basis. contribution of working group i to the sixth assessment report of the intergovernmental panel on climate change.* Cambridge University Press, Cambridge, United Kingdom and New York, NY, USA. doi: 10.1017/9781009157896.004

Hao, Z., Hao, F., Singh, V. P., & Zhang, X. (2018). Changes in the severity of compound drought and hot extremes over global land areas. *Environmental Research Letters*, *13*(12), 124022. Retrieved from https://dx.doi.org/10.1088/1748-9326/aaee96 doi: 10.1088/1748-9326/aaee96

Hauser, M., Engelbrecht, F., & Fischer, E. M. (2022). *Transient global warming levels for CMIP5 and CMIP6.* Zenodo. Retrieved from https://doi.org/10.5281/zenodo.7390473 doi: 10.5281/zenodo.7390473

Jha, S., Gudmundsson, L., & Seneviratne, S. I. (2023). Partitioning the uncertainties in compound hot and dry precipitation, soil moisture, and runoff extremes projections in cmip6. *Earth's Future*, *11*(3), e2022EF003315. Retrieved from https://agupubs.onlinelibrary.wiley.com/doi/abs/10.1029/2022EF003315 (e2022EF003315 2022EF003315) doi: https://doi.org/10.1029/2022EF003315

Kirchmeier-Young, M. C., Zwiers, F. W., & Gillett, N. P. (2017). Attribution of extreme events in arctic sea ice extent. *Journal of Climate*, *30*(2), 553 - 571. Retrieved from https://journals.ametsoc.org/view/journals/clim/30/2/jcli-d-16-0412.1.xml doi: https://doi.org/10.1175/JCLI-D-16-0412.1

Kornhuber, K., Osprey, S., Coumou, D., Petri, S., Petoukhov, V., Rahmstorf, S., & Gray, L. (2019). Extreme weather events in early summer 2018 connected by a recurrent hemispheric wave-7 pattern. *Environmental Research Letters*, *14*(5), 054002. Retrieved from https://doi.org/10.1088/1748-9326/ab13bf doi: 10.1088/1748-9326/ab13bf

Leduc, M., Mailhot, A., Frigon, A., Martel, J.-L., Ludwig, R., Brietzke, G. B., ... Scinocca, J. (2019). The climex project: A 50-member ensemble of climate change projections at 12-km resolution over europe and northeastern north america with the canadian regional climate model (crcm5). *Journal of Applied Meteorology and Climatology*, *58*(4), 663–693. doi: 10.1175/JAMC-D-18-0021.1

Leonard, M., Westra, S., Phatak, A., Lambert, M., van den Hurk, B., McInnes, K., ... Stafford-Smith, M. (2014). A compound event framework for understanding extreme impacts. *WIREs Climate Change*, *5*(1), 113-128. Retrieved from https://wires.onlinelibrary.wiley.com/doi/abs/10.1002/wcc.252 doi: https://doi.org/10.1002/wcc.252

Lesk, C., Rowhani, P., & Ramankutty, N. (2016). Influence of extreme weather disasters on global crop production. *Nature*, *529*, 84–87. Retrieved from https://doi.org/10.1038/nature16467 doi: 10.1038/nature16467

Li, H., Keune, J., Smessaert, F., Nieto, R., Gimeno, L., & Miralles, D. G. (2023). Land–atmosphere feedbacks contribute to crop failure in global rainfed breadbaskets. *npj Climate and Atmospheric Science*, *6*, 51. Retrieved from https://doi.org/10.1038/s41612-023-00375-6 doi: 10.1038/s41612-023-00375-6

Liu, P. R., & Raftery, A. E. (2021). Country-based rate of emissions reductions should increase by 80% beyond nationally determined contributions to meet the 2 °c target. *Communications Earth & Environment*, *2*, 29. Retrieved from https://doi.org/10.1038/s43247-021-00097-8 doi: 10.1038/s43247-021-00097-8

Maher, N., Milinski, S., & Ludwig, R. (2021). Large ensemble climate model simulations: introduction, overview, and future prospects for utilising multiple types of large ensemble. *Earth System Dynamics*, *12*(2), 401–418. Retrieved from https://esd.copernicus.org/articles/12/401/2021/ doi: 10.5194/esd-12-401-2021

Manning, C., Widmann, M., Bevacqua, E., Loon, A. F. V., Maraun, D., & Vrac, M. (2019). Increased probability of compound long-duration dry and hot events in europe during summer (1950–2013). *Environmental Research Letters*, *14*(9), 094006. Retrieved from https://dx.doi.org/10.1088/1748-9326/ab23bf doi: 10.1088/1748-9326/ab23bf

Markonis, Y., Kumar, R., Hanel, M., Rakovec, O., Máca, P., & AghaKouchak, A. (2021). The rise of compound warm-season droughts in europe. *Science Advances*, *7*(6), eabb9668. Retrieved from https://www.science.org/doi/abs/10.1126/sciadv.abb9668 doi: 10.1126/sciadv.abb9668

Miller, J., Böhnisch, A., Ludwig, R., & Brunner, M. I. (2023). Climate change impacts on regional fire weather in heterogeneous landscapes of central europe. *Natural Hazards and Earth System Sciences Discussions*, *2023*, 1–25. Retrieved from https://nhess.copernicus.org/preprints/nhess-2023-51/ doi: 10.5194/nhess-2023-51

Miralles, D. G., Gentine, P., Seneviratne, S. I., & Teuling, A. J. (2019). Land–atmospheric feedbacks during droughts and heatwaves: state of the science and current challenges. *Annals of the New York Academy of Sciences*, *1436*(1), 19-35. Retrieved from https://nyaspubs.onlinelibrary.wiley.com/doi/abs/10.1111/nyas.13912 doi: https://doi.org/10.1111/nyas.13912

Mukherjee, S., & Mishra, A. K. (2021). Increase in compound drought and heatwaves in a warming world. *Geophysical Research Letters*, *48*(1), e2020GL090617. Retrieved from https://agupubs.onlinelibrary.wiley.com/doi/abs/10.1029/2020GL090617 (e2020GL090617 2020GL090617) doi: https://doi.org/10.1029/2020GL090617

Mukherjee, S., Mishra, A. K., Zscheischler, J., & Entekhabi, D. (2023). Interaction between dry and hot extremes at a global scale using a cascade modeling framework. *Nature Communications*, *14*, 277. Retrieved from https://doi.org/10.1038/s41467-022-35748-7 doi: 10.1038/s41467-022-35748-7

Nagler, T., Schepsmeier, U., Stoeber, J., Brechmann, E. C., Graeler, B., Erhardt, T., ... Vatter, T. (2023). *Vinecopula: Statistical inference of vine copulas. r package version 2.4.5.* Retrieved from https://github.com/tnagler/VineCopula

O, S., Bastos, A., Reichstein, M., Li, W., Denissen, J., Graefen, H., & Orth, R. (2022). The role of climate and vegetation in regulating drought–heat extremes. *Journal of Climate*, *35*(17), 5677 - 5685. Retrieved from https://journals.ametsoc.org/view/journals/clim/35/17/JCLI-D-21-0675.1.xml

817 doi: https://doi.org/10.1175/JCLI-D-21-0675.1
818 Poschlod, B., Zscheischler, J., Sillmann, J., Wood, R. R., & Ludwig, R. (2020). Cli-
819 mate change effects on hydrometeorological compound events over southern
820 norway. *Weather and Climate Extremes*, *28*, 100253. Retrieved from `https://`
821 `www.sciencedirect.com/science/article/pii/S2212094719301574` doi:
822 https://doi.org/10.1016/j.wace.2020.100253
823 Richardson, M. I., Cowtan, K. D., Hawkins, E., & Stolpe, M. B. (2016). Rec-
824 onciled climate response estimates from climate models and the energy
825 budget of earth. *Nature Climate Change*, *6*, 931-935. Retrieved from
826 `https://doi.org/10.1038/nclimate3066` doi: 10.1038/nclimate30660
827 Rousi, E., Fink, A. H., Andersen, L. S., Becker, F. N., Beobide-Arsuaga, G., Breil,
828 M., ... Xoplaki, E. (2023). The extremely hot and dry 2018 summer in central
829 and northern europe from a multi-faceted weather and climate perspective.
830 *Natural Hazards and Earth System Sciences*, *23*(5), 1699–1718. Retrieved
831 from `https://nhess.copernicus.org/articles/23/1699/2023/` doi:
832 10.5194/nhess-23-1699-2023
833 Salvadori, G., Durante, F., De Michele, C., Bernardi, M., & Petrella, L. (2016). A
834 multivariate copula-based framework for dealing with hazard scenarios and
835 failure probabilities. *Water Resources Research*, *52*(5), 3701-3721. Retrieved
836 from `https://agupubs.onlinelibrary.wiley.com/doi/abs/10.1002/`
837 `2015WR017225` doi: https://doi.org/10.1002/2015WR017225
838 Schwalm, C. R., Glendon, S., & Duffy, P. B. (2020). Rcp8.5 tracks cumulative
839 co¡sub¿2¡/sub¿ emissions. *Proceedings of the National Academy of Sciences*,
840 *117*(33), 19656-19657. Retrieved from `https://www.pnas.org/doi/abs/`
841 `10.1073/pnas.2007117117` doi: 10.1073/pnas.2007117117
842 Schwingshackl, C., Hirschi, M., & Seneviratne, S. I. (2017). Quantifying spa-
843 tiotemporal variations of soil moisture control on surface energy balance and
844 near-surface air temperature. *Journal of Climate*, *30*(18), 7105 - 7124. Re-
845 trieved from `https://journals.ametsoc.org/view/journals/clim/30/18/`
846 `jcli-d-16-0727.1.xml` doi: https://doi.org/10.1175/JCLI-D-16-0727.1
847 Seneviratne, S., Zhang, X., Adnan, M., Badi, W., Dereczynski, C., Di Luca, A., ...
848 Zhou, B. (2021). Weather and climate extreme events in a changing climate.
849 In V. Masson-Delmotte et al. (Eds.), *Climate change 2021: The physical sci-*
850 *ence basis. contribution of working group i to the sixth assessment report of the*
851 *intergovernmental panel on climate change.* doi: 10.1017/9781009157896.013
852 Swart, N. C., Cole, J. N. S., Kharin, V. V., Lazare, M., Scinocca, J. F., Gillett,
853 N. P., ... Winter, B. (2019). The canadian earth system model version 5
854 (canesm5.0.3). *Geoscientific Model Development*, *12*(11), 4823–4873. Re-
855 trieved from `https://gmd.copernicus.org/articles/12/4823/2019/` doi:
856 10.5194/gmd-12-4823-2019
857 Teuling, A. J., Hirschi, M., Ohmura, A., Wild, M., Reichstein, M., Ciais, P., ...
858 Seneviratne, S. I. (2009). A regional perspective on trends in continental
859 evaporation. *Geophysical Research Letters*, *36*(2). Retrieved from `https://`
860 `agupubs.onlinelibrary.wiley.com/doi/abs/10.1029/2008GL036584` doi:
861 https://doi.org/10.1029/2008GL036584
862 Toreti, A., Belward, A., Perez-Dominguez, I., Naumann, G., Luterbacher, J., Cronie,
863 O., ... Zampieri, M. (2019). The exceptional 2018 european water seesaw
864 calls for action on adaptation. *Earth's Future*, *7*(6), 652-663. Retrieved
865 from `https://agupubs.onlinelibrary.wiley.com/doi/abs/10.1029/`
866 `2019EF001170` doi: https://doi.org/10.1029/2019EF001170
867 Trenberth, K. E., & Shea, D. J. (2005). Relationships between precipitation and
868 surface temperature. *Geophysical Research Letters*, *32*(14). Retrieved
869 from `https://agupubs.onlinelibrary.wiley.com/doi/abs/10.1029/`
870 `2005GL022760` doi: https://doi.org/10.1029/2005GL022760
871 UNFCCC. (2015). *Adoption of the paris agreement. report no.*

fccc/cp/2015/l.9/rev.1. Retrieved from http://unfccc.int/resource/docs/2015/cop21/eng/l09r01.pdf

Vogel, M. M., Zscheischler, J., Wartenburger, R., Dee, D., & Seneviratne, S. I. (2019). Concurrent 2018 hot extremes across northern hemisphere due to human-induced climate change. *Earth's Future*, *7*(7), 692-703. Retrieved from https://agupubs.onlinelibrary.wiley.com/doi/abs/10.1029/2019EF001189 doi: https://doi.org/10.1029/2019EF001189

von Trentini, F., Leduc, M., & Ludwig, R. (2019). Assessing natural variability in RCM signals: comparison of a multi model EURO-CORDEX ensemble with a 50-member single model large ensemble. *Climate Dynamics*, *53*, 1963-1979. Retrieved from https://doi.org/10.1007/s00382-019-04755-8 doi: 10.1007/s00382-019-04755-8

Wang, R., Lü, G., Ning, L., Yuan, L., & Li, L. (2021). Likelihood of compound dry and hot extremes increased with stronger dependence during warm seasons. *Atmospheric Research*, *260*, 105692. Retrieved from https://www.sciencedirect.com/science/article/pii/S0169809521002489 doi: https://doi.org/10.1016/j.atmosres.2021.105692

Zink, M., Samaniego, L., Kumar, R., Thober, S., Mai, J., Schäfer, D., & Marx, A. (2016). The german drought monitor. *Environmental Research Letters*, *11*(7), 074002. Retrieved from https://dx.doi.org/10.1088/1748-9326/11/7/074002 doi: 10.1088/1748-9326/11/7/074002

Zscheischler, J., & Fischer, E. M. (2020). The record-breaking compound hot and dry 2018 growing season in germany. *Weather and Climate Extremes*, *29*, 100270. Retrieved from https://www.sciencedirect.com/science/article/pii/S2212094719302002 doi: https://doi.org/10.1016/j.wace.2020.100270

Zscheischler, J., Martius, O., Westra, S., Bevacqua, E., Raymond, C., Horton, R. M., ... Vignotto, E. (2020). A typology of compound weather and climate events. *Nature Reviews Earth & Environment*, *1*, 333–347. Retrieved from https://doi.org/10.1038/s43017-020-0060-z doi: 10.1038/s43017-020-0060-z

Zscheischler, J., Orth, R., & Seneviratne, S. I. (2015). A submonthly database for detecting changes in vegetation-atmosphere coupling. *Geophysical Research Letters*, *42*(22), 9816-9824. Retrieved from https://agupubs.onlinelibrary.wiley.com/doi/abs/10.1002/2015GL066563 doi: https://doi.org/10.1002/2015GL066563

Zscheischler, J., & Seneviratne, S. I. (2017). Dependence of drivers affects risks associated with compound events. *Science Advances*, *3*(6), e1700263. Retrieved from https://www.science.org/doi/abs/10.1126/sciadv.1700263 doi: 10.1126/sciadv.1700263